THE JOURNAL OF BIOLOGICAL CHEMISTRY VOL. 283, NO. 2, pp. 1113–1119, January 11, 2008

The Structure of the Yeast Plasma Membrane SNARE Complex Reveals Destabilizing Water-filled Cavities*

Received for publication, September 21, 2007, and in revised form, October 22, 2007 Published, JBC Papers in Press, October 22, 2007, DOI 10.1074/jbc.M707912200

Pavel Strop, Stephen E. Kaiser, Marija Vrljic, and Axel T. Brunger[1]

From the Howard Hughes Medical Institute and Departments of Molecular and Cellular Physiology, Neurology and Neurological Sciences, Structural Biology, and Photon Science, Stanford University, Stanford, California 94305

SNARE proteins form a complex that leads to membrane fusion between vesicles, organelles, and plasma membrane in all eukaryotic cells. We report the 1.7 Å resolution structure of the SNARE complex that mediates exocytosis at the plasma membrane in the yeast *Saccharomyces cerevisiae*. Similar to its neuronal and endosomal homologues, the *S. cerevisiae* SNARE complex forms a parallel four-helix bundle in the center of which is an ionic layer. The *S. cerevisiae* SNARE complex exhibits increased helix bending near the ionic layer, contains water-filled cavities in the complex core, and exhibits reduced thermal stability relative to mammalian SNARE complexes. Mutagenesis experiments suggest that the water-filled cavities contribute to the lower stability of the *S. cerevisiae* complex.

Membrane fusion is a fundamental and highly regulated process that is required for the transport of proteins, lipids, and metabolites in all eukaryotes. Highly conserved SNARE[2] (soluble *N*-ethylmaleimide-sensitive factor attachment protein receptor) proteins play a key role in the fusion of a transport vesicle with its target membrane (1, 2). Specific sets of SNAREs located on vesicle and target membranes form a complex that draws together SNARE transmembrane domains, leading to juxtaposition and fusion of the two lipid membranes. SNARE-mediated fusion processes are either constitutive or triggered, and they require additional SNARE-interacting factors, such as Munc13, Sec1/Munc 18-like proteins, synaptotagmins, and complexins (3, 4).

Neuronal SNAREs play a key role in the fusion of synaptic vesicles with the plasma membrane, a process that is critical for neurotransmission (5). Synaptic vesicles dock at the plasma membrane and upon cell depolarization and Ca^{2+} entry fuse with the plasma membrane, thus releasing neurotransmitters into the synaptic cleft. The neuronal SNARE complex is composed of synaptobrevin 2, which is primarily localized to synaptic vesicles, and syntaxin 1A and SNAP-25, which are primarily associated with the plasma membrane.

The family of yeast SNAREs mediates constitutive fusion between transport vesicles and intracellular organelles or the plasma membrane (6, 7). Yeast has been a valuable system for studying membrane fusion and vesicular transport because of the ease of genetic and biochemical manipulations. Yeast is also one of the first organisms that evolved to utilize intracellular membrane fusion and therefore provides a valuable snapshot of the fusion machinery in lower eukaryotes. The *Saccharomyces cerevisiae* SNARE proteins involved in exocytosis at the plasma membrane (the synaptobrevin homologue Snc1p, the syntaxin homologue Sso1p, and the SNAP-25 homologue Sec9p) show assembly properties similar to their neuronal and endosomal homologues. Relative to the neuronal SNARE complex the *S. cerevisiae* SNARE complex exhibits decreased thermal stability, and prior to SNARE complex formation, Sso1p interacts with Sec9p with 1:1 stoichiometry (as opposed to a mixture of 1:1 and 1:2 for the neuronal SNAREs) (8, 9).

Several structures of neuronal SNARE complexes and endosomal SNARE complexes have been solved from higher eukaryotes (10–13); however, no structural information is available for lower eukaryotes. To dissect the differences between *S. cerevisiae*, neuronal, and endosomal SNARE complexes we determined the structure of the *S. cerevisiae* plasma membrane SNARE complex consisting of the cytoplasmic SNARE core domains at 1.7 Å resolution. Surprisingly, we found a larger number of buried water molecules compared with the neuronal SNARE complex. We then performed mutagenesis experiments to determine the influence of these water molecules on the stability of the complex.

EXPERIMENTAL PROCEDURES

Protein Expression and Purification—The SNARE core domains of Snc1p (residues 28–92), Sso1p (residues 189–257), Sec9p (residues 429–500), and Sec9p (residues 589–651) were cloned into the pet28b vector (Novagen) with an N-terminal His_6 tag. All proteins were transformed into *Escherichia coli* BL21DE3 cells and grown at 37 °C until an optical density (measured at 600 nm) of 1.0 was reached. Protein expression was induced with 0.5 mM isopropyl-1-thio-β-D-galactopyranoside at 37 °C for 1–3 h. Cells were harvested by centrifugation and frozen in liquid nitrogen.

For purification, cells were resuspended in lysis buffer (100 mM Tris, pH 8.0, 6 M GdHCl) and lysed by sonication. Lysate was incubated in the lysis buffer for 1 h and then cleared by ultracentrifugation before incubation with nickel-nitrilotriacetic acid resin for 4 h. The resin was washed with 250 ml of lysis buffer, and proteins were eluted in 50 mM Tris, pH 8.0, 150 mM NaCl, and 200 mM GdHCl. Ssop1 protein was prone to aggregation and thus the buffer was supplemented with 1.5 M urea.

* The costs of publication of this article were defrayed in part by the payment of page charges. This article must therefore be hereby marked "*advertisement*" in accordance with 18 U.S.C. Section 1734 solely to indicate this fact.
The atomic coordinates and structure factors (code 3B5N) have been deposited in the Protein Data Bank, Research Collaboratory for Structural Bioinformatics, Rutgers University, New Brunswick, NJ (http://www.rcsb.org/).
[1] To whom correspondence should be addressed. Tel.: 650-736-1809; Fax: 650-736-1961; E-mail: brunger@stanford.edu.
[2] The abbreviations used are: SNARE, soluble *N*-ethylmaleimide-sensitive factor attachment protein receptor; MES, 4-morpholineethanesulfonic acid.

TABLE 1
Refinement and model statistics

Space group	$P2_1$
Cell dimensions	
a, b, c (Å)	76.9, 48.1, 110.3
Resolution (Å)	50.0-1.7
Measured reflections	313206
Unique reflections	90852
R_{merge}	4.5 (28.2)
Completeness (%)	94.0 (66.0)
$I/\sigma(I)$	23 (3.1)
Number of protein atoms	6064
Water molecules	592
Overall B factor value (Å^2)	27.5
R_{cryst}	20.7
R_{free}	24.7
Root mean square deviation	
Bonds	0.007
Angles	0.78
Ramachandran	
Most favored regions	99.8
Additional allowed regions	0.2
Generously allowed regions	0.0
Disallowed regions	0.0

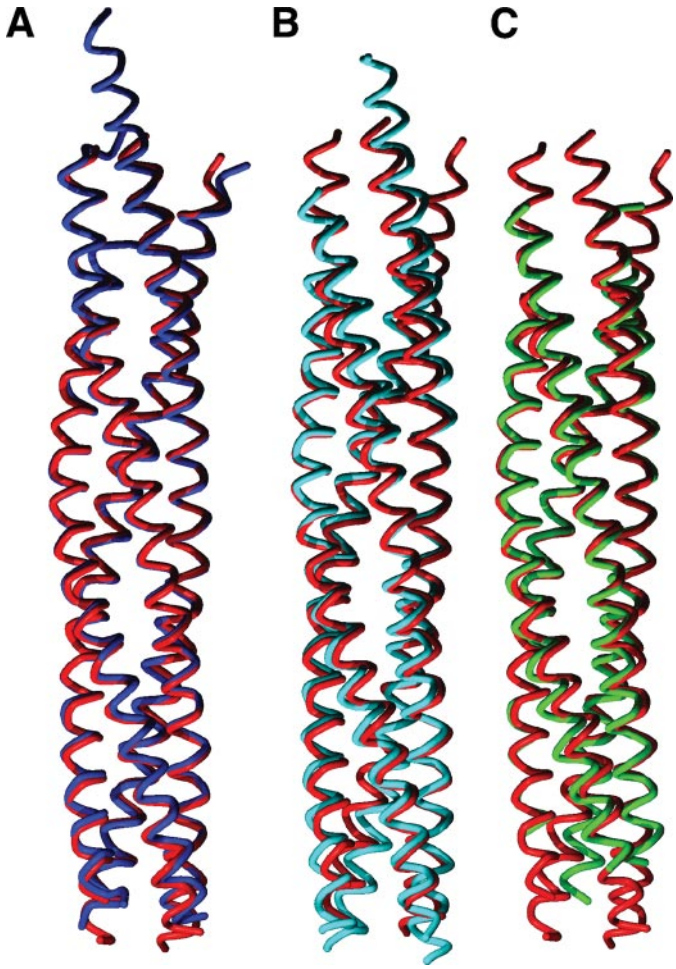

FIGURE 1. **Superposition of the *S. cerevisiae*, neuronal, and endosomal SNARE complexes.** *A*, superposition of the *S. cerevisiae* (*red*) and neuronal (*blue*, PDB code 1N7S) plasma membrane SNARE complexes. *B*, superposition of the *S. cerevisiae* plasma membrane (*red*) and early endosomal (*cyan*) (PDB code 2NPS) SNARE complexes. *C*, superposition of the *S. cerevisiae* plasma membrane (*red*) and late endosomal (*green*) (PDB code 2GL2) SNARE complexes. Figs. 1, 2, 3, and 6 were made with POVSCRIPT (25); Fig. 5 was made with PyMOL (26).

His_6 tags were removed by thrombin cleavage at room temperature for 2 h, and cleavage was verified by mass spectrometry.

Complex Formation—The ternary complex was assembled by mixing Snc1p, Ssop1, Sec9p (residues 429–500), and Sec9p (residues 589–651) at a 1:1:1:1 molar ratio in 6 M GdHCl, followed by overnight dialysis into 50 mM Hepes, pH 7.5, 250 mM NaCl. After dialysis, the *S. cerevisiae* SNARE complex was diluted to 75 mM NaCl and purified by MonoQ ion exchange chromatography followed by size exclusion chromatography on a Superdex75 16/60 column in 50 mM Hepes, pH 7.5, 150 mM NaCl.

Crystallization, Data Collection, and Refinement—*S. cerevisiae* SNARE complex crystals were grown by the hanging drop method at 25 °C using a precipitant solution containing 100 mM MES, pH 6.25, 30% 2-methyl-2,4-pentanediol, 200 mM sodium bromide. Square-shaped crystals appeared in a few days and grew to ~200 × 200 × 200 μm. Crystals were directly flash frozen in liquid nitrogen. Diffraction data were collected at Stanford Synchrotron Radiation Laboratory (SSRL) beamline 11–1. The crystals belong to the space group $P2_1$ with unit cell dimensions a = 76.9 Å, b = 48.11 Å, c = 110.3 Å, and $\beta = 97.7°$ and diffracted to 1.7 Å resolution (Table 1). All diffraction data were processed with DENZO and SCALEPACK (14).

A polyalanine model of the neuronal SNARE complex (Protein Data Bank code 1N7S) was used for a molecular replacement search in PHASER (15). Three copies of the *S. cerevisiae* SNARE complex were located in the asymmetric unit. Alternate cycles of model building using the program COOT (16), positional, TLS, and individual restrained thermal factor refinement in the Crystallography and NMR System 1.2 (CNS) (17, 27), and PHENIX (18) and addition of water molecules reduced the *R* and free *R* values to 20.7 and 24.7%, respectively, for all of the reflections (1.6 Å resolution). A total of 99.8% of the residues in *S. cerevisiae* SNARE complex are in the most favored regions of the Ramachandran plot, and 0.2% in the additional allowed regions as calculated with PROCHECK (19). The final model contains 6656 atoms (6064 protein and 592 waters). The coordinates for the structure have been deposited in the Protein Data Bank.

Mutagenesis—The removal of the first cavity was accomplished by a single mutation in Sec9p (T615M). The cavity 2 mutant consists of two mutations, T39V in Snc1p and S605I in Sec9p. The cavity 3 mutant has a single mutation in Sec9p (N486M). The removal of all three cavities was achieved by four combined mutations (T39V in Snc1p, and N486M, S605I, and T615M in Sec9p).

CD Analysis—CD data were collected on an Aviv 202–01 spectrometer equipped with a thermoelectric unit using a 1-mm-path length cell. Protein samples were 50 μM in buffer containing 25 mM sodium phosphate, pH 7.5, and 150 mM KCl. Protein concentrations were determined by UV spectrophotometry at 280 nm and BCA assay (Pierce). Thermal melts were monitored at 222 nm. Data were collected every 2 °C with an equilibration time of 2 min and an averaging time of 15 s. All

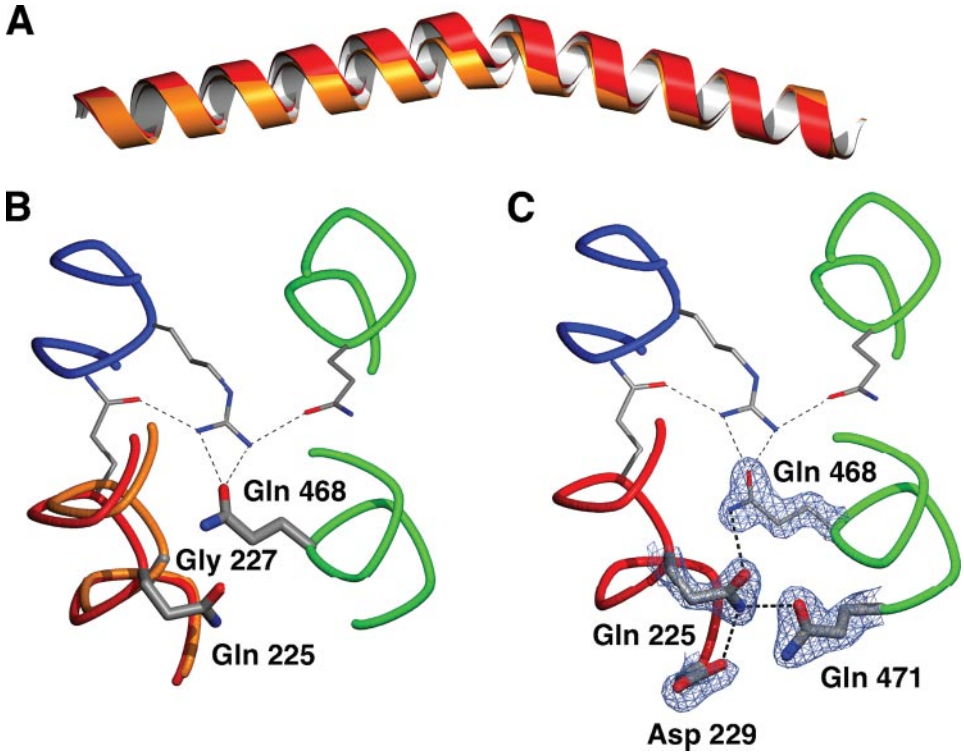

FIGURE 2. **Helix bending near the ionic layer in the *S. cerevisiae* plasma membrane SNARE complex.** *A*, ribbon diagram of the superposition of *S. cerevisiae* Sso1p (*red*) and neuronal syntaxin 1A (*orange*), showing the increase in the helix bending of Sso1p in the *S. cerevisiae* SNARE complex. *B*, close-up of the region near Gln-225. The syntaxin 1A helix is shown in *orange*, Sso1p in *red*, Snc1p in *blue*, and Sec9p in *green*. The distances between the C_α position of Gly-227 in syntaxin 1A and the C_α positions of Gln-225 in the three *S. cerevisiae* SNARE complexes in the asymmetric unit are 1.0, 1.4, and 1.7 Å, respectively. Gly-227 is the syntaxin 1A residue equivalent to Gln-225 in *S. cerevisiae* Sso1p. *C*, simulated annealing σ_A-weighted omit map contoured at 3 σ of residues forming a hydrogen bond network with Gln-225 in Sso1p. Color coding is as in *panel B*. Ionic layer residues are shown in *thin sticks*, whereas other residues interacting with Gln-225 are shown as *thicker sticks* with their electron density superimposed.

temperature melts were performed at least four times and averaged.

RESULTS AND DISCUSSION

Although the level of sequence identity between neuronal and *S. cerevisiae* SNAREs is not exceptionally high (Snc1p and synaptobrevin 2 (36%), Sso1p and syntaxin 1A (50%), and Sec9p and SNAP-25A (32%)), the overall structure of the *S. cerevisiae* SNARE complex is very similar to that of neuronal and endosomal SNARE complexes (Fig. 1). All structures consist of a four-helix bundle with all four helices arranged in parallel, *i.e.* their N and C termini are aligned and there is an ionic layer composed of one arginine and three glutamine residues at the center of the complex. Interestingly, the structures of SNARE complexes that are involved in plasma membrane fusion (the neuronal and *S. cerevisiae* SNARE complexes) are more similar to one another than they are to the endosomal SNARE complexes; the root mean square deviations between *S. cerevisiae*, and neuronal, early endosomal, and late endosomal structures are 0.9, 2.3, and 1.4 Å, respectively.

A striking difference between the neuronal and *S. cerevisiae* SNARE complexes is a more pronounced helical bend near the ionic layer (Fig. 2*A*). This increased bend is likely caused by the glycine to glutamine (Gln-225) substitution in Sso1p. The larger side chain in the *S. cerevisiae* SNARE complex would clash with Gln-468 (one of the three ionic layer glutamines) if it had the conformation of the neuronal complex. Therefore, the backbone of Sso1p near residue 225 is pushed 1.0–1.7 Å away from the ionic layer (Fig. 2*B*; note the hydrogen bonding network involving Gln-225 in Fig. 2*C*), causing the more pronounced bending of the Sso1p helix. The degree of bending varies between the three independent *S. cerevisiae* SNARE complexes in the asymmetric unit, suggesting that this region of the *S. cerevisiae* SNARE complex is flexible in solution.

To investigate the contribution of the Sso1p bending to the stability of the *S. cerevisiae* SNARE complex, we created a Q225G mutant of Sso1p. The Q225G mutant should allow the *S. cerevisiae* SNARE complex to form a complex with a less pronounced bend at the ionic layer. However, the mutation decreased the thermal stability of the complex by 2 °C (not shown), suggesting that the increased bending angle of Sso1p is not destabilizing.

Interestingly, residue Gly-227 in syntaxin 1A (equivalent to Gln-225 in *S. cerevisiae* Sso1p), which does not induce bending of the neuronal SNARE complex, is almost entirely conserved among syntaxins involved in plasma membrane fusion and in endosome/lysosome fusion (Syntaxins 1A, 2, 3, 4, 7, 12, and 16). It is, however, variable in Golgi, endoplasmic reticulum, and yeast syntaxins, where its identity varies. It is difficult to directly compare the differences in bending between *S. cerevisiae* and endosomal SNARE complexes due to increasing differences in helix position, especially toward the SNARE complex termini. The endosomal SNARE complexes, like the neuronal SNARE complex, have a glycine at residue 227 (residue 225 in neuronal syntaxin 1A). Inspection of the structures suggests that the degree to which the syntaxin helix is pushed out is governed by the size of side chains in the +1 layer.

Apart from the increased bending of the Sso1p helix at the ionic layer, the ionic layer of *S. cerevisiae* SNAREs is very similar to that of the neuronal SNARE complex (Fig. 3, *A* and *B*), where Arg-53 forms a hydrogen bond network with Gln-224, Gln-468, and Gln-622 of Sso1p and Sec9p (Fig. 3*A*). The side chain of Arg-53 adopts two different rotamers in the three independent *S. cerevisiae* SNARE complexes in the asymmetric unit. Alternative rotamers of the equivalent arginine residue in the ionic layer have also been observed in neuronal SNAREs (10).

One remarkable property of the neuronal SNARE complex is its high stability: The neuronal SNARE complex undergoes cooperative unfolding with a melting temperature of ~90 °C

(Fig. 4) and resists SDS denaturation up to 60 °C (10). The *S. cerevisiae* SNARE complex is less stable and melts at T_m = 55 °C (Fig. 4), nearly 35 °C lower than its neuronal homologue. In addition to its lower T_m, the *S. cerevisiae* SNARE complex is not SDS-resistant. The early and late endosomal SNARE complexes have melting temperatures of 87 (12) and 78 °C, respectively (20).

The melting temperature of the *S. cerevisiae* SNARE complex increases with the length of the constructs from 55 to 64 °C when an additional eight residues are included at the N terminus of the complex (data not shown). Similar behavior was observed for the neuronal complex, where the T_m increases from 90 to 95 °C (10). The longer, more thermally stable *S. cerevisiae* SNARE complex, however, diffracted only to ~3.5 Å resolution and was not pursued further. Similarly, the longer neuronal SNARE complex was solved at 2.4 Å resolution (11), whereas the shorter complex diffracted to 1.45 Å (10). The effect of SNARE complex length is further exemplified by our previous report (9). The melting temperature of the *S. cerevisiae* SNARE complex consisting of Sso1p N-terminal domain (residues 1–265), Snc1p (residues 1–93), and Sec9p (residues 401–651) is 71 °C (9), whereas the *S. cerevisiae* SNARE complex described here (Snc1p (residues 28–92), Sso1p (residues 189–257), Sec9p (residues 429–500), and Sec9p (residues 589–651)) has a reduced melting temperature of 55 °C. Therefore, the N terminus of Sso1p, length of the *S. cerevisiae* SNARE complex, or the linker between the two Sec9p helices can have a large effect on complex thermal stability. For these reasons, the comparison of the *S. cerevisiae* and neuronal SNARE complexes was carried out with the shorter neuronal SNARE complex that has nearly identical length (except for the SN1 fragment, which has eleven more residues at the N terminus). The early endosomal complex is also of similar length to the *S. cerevisiae*

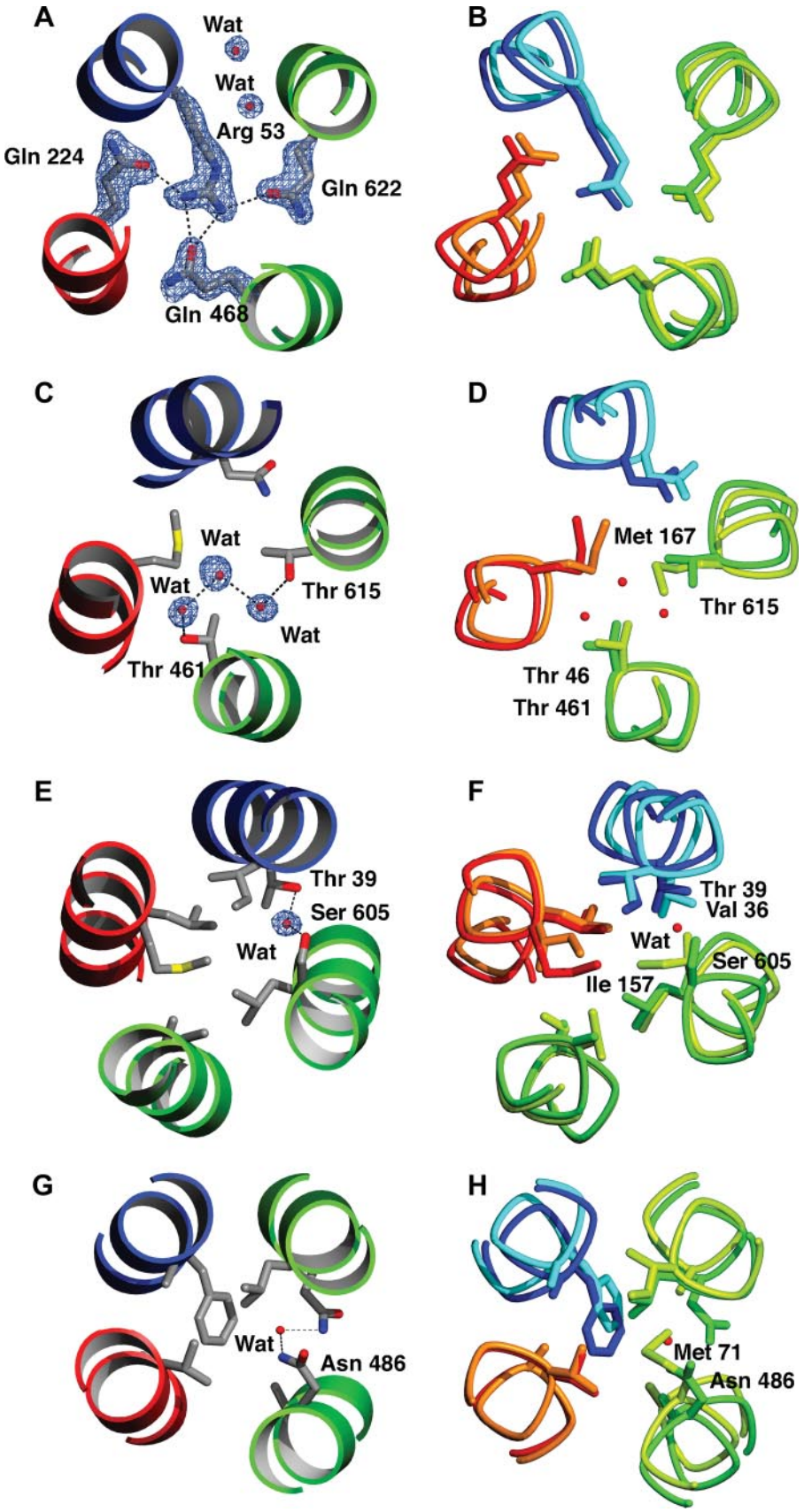

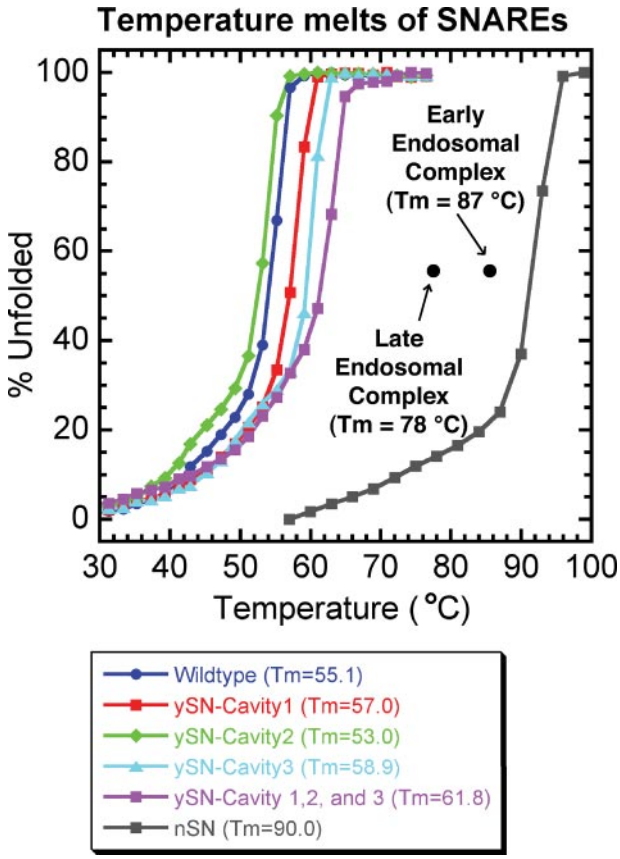

FIGURE 4. **Temperature melts of neuronal and *S. cerevisiae* plasma membrane SNARE complexes.** The neuronal SNARE complex is shown as *gray squares* (T_m = 90 °C), and the wild type *S. cerevisiae* SNARE complex is shown as *blue circles* (T_m = 55 °C). Early and late endosomal SNARE complex melting temperatures are also shown for comparison (T_m = 87 and 78 °C, respectively). Temperature melts of *S. cerevisiae* SNARE mutants are shown as follows: Cavity 1 mutant (Sec9p T615M), *red* (T_m = 57 °C); cavity 2 mutant (Snc1p T39V and Sec9p S6O5I), *green* (T_m = 53 °C); cavity 3 mutant (Sec9p N468M), *cyan* (T_m = 58.9 °C); all mutations combined, *purple squares* (T_m = 61.8 °C).

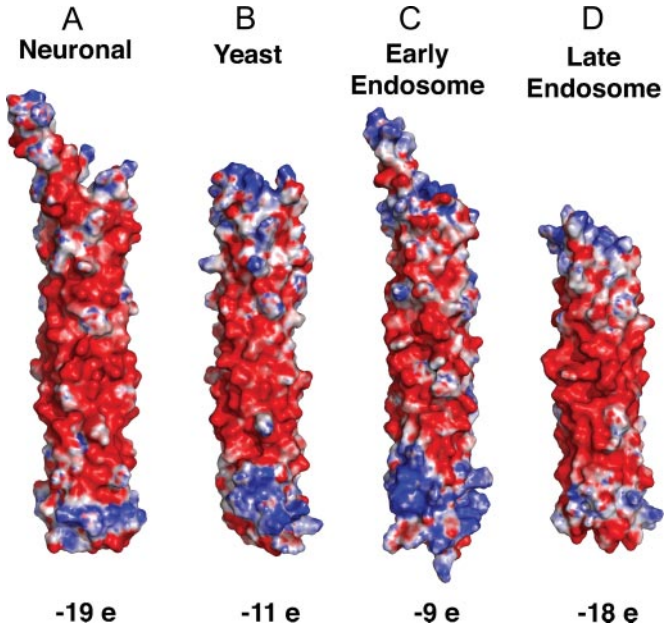

FIGURE 5. **Electrostatic potential surfaces of SNARE complexes.** *A*, neuronal SNARE complex (PDB code 1N7S). *B*, *S. cerevisiae* SNARE complex. *C*, early endosomal SNARE complex (PDB code 2NPS). *D*, late endosomal SNARE complex (PDB code 1GL2). The electrostatic potential surfaces were generated in APBS and are all contoured from −10 k_BT (*red*) to +10 k_BT (*blue*). The figure was generated in PyMOL.

SNARE complex, whereas the late endosomal complex is shorter at both N and C termini.

The core of the *S. cerevisiae* SNARE complex contains several unusual layers that may contribute to its lower stability. For example, the neuronal SNARE complex has a methionine in the −2 layer (Met-167 in SNAP-25), whereas the *S. cerevisiae* Sec9p has a threonine (Fig. 3, *C* and *D*). The smaller side chain of Thr-615 allows water to penetrate the center of the SNARE complex, creating an internal water-filled cavity. Indeed, three ordered water molecules are present in this layer (Fig. 3*C*). These water molecules form hydrogen bonds to each other and to Thr-461 and Thr-615 of Sec9p.

A second water-filled cavity is formed between the −4 and −5 layers in the *S. cerevisiae* SNARE complex (Fig. 3, *E* and *F*). The presence of a water molecule at this position is made possible by a hydrophobic to hydrophilic change of two residues compared to the neuronal SNARE complex: Val-36 in synaptobrevin 2 and Ile-157 in SNAP-25A *versus* Thr-39 in Snc1p and Ser-605 in Sec9p (Fig. 3*F*). The water molecule is held in place by forming hydrogen bonds to both Thr-39 in Snc1p and Ser-605 in Sec9p (Fig. 3*E*).

A third cavity is present between the +5 and +6 layers. The cavity is created by a change of methionine in SNAP-25 (Met-71) to an asparagine residue (Asn-486) in the *S. cerevisiae* SNARE complex. The water molecule in this cavity is not present in all three complexes in the asymmetric unit and most likely is only partially occupied. In addition, two distinct conformations of Asn-486 can be seen in one of the three complexes, suggesting loose packing and conformational variability in the +5 and +6 layers.

Comparison of all SNARE complex structures determined at high resolution (2 Å or higher) showed that the *S. cerevisiae* SNARE complex has the most water-filled cavities. To estimate the destabilizing effect of water-filled cavities in the *S. cerevisiae* SNARE complex, we mutated residues in these layers to match those found in the neuronal complex, which contain no water-filled cavities. Separate removal of cavities 1 and 3 stabilizes the *S. cerevisiae* SNARE complex by 1.9 and 3.8 °C, respectively, whereas removal of cavity 2 destabilizes the SNARE complex by

FIGURE 3. **Comparison of the central ionic layer and −2, −4/−5, and +5/+6 layers of *S. cerevisiae* and neuronal plasma membrane SNARE complexes.** Snc1p is shown in *blue*, Ssop in *red*, Sec9p in *green*, synaptobrevin 2 in *cyan*, syntaxin 1A in *orange*, and SNAP-25A in *yellow*. Hydrogen bonds are shown as *dashed lines*. *A*, simulated annealing omit map contoured at 3 σ of the ionic layer in the *S. cerevisiae* SNARE complex. *B*, superposition of the ionic layers of the *S. cerevisiae* and neuronal SNARE complexes. *C*, simulated annealing omit map contoured at 3 σ of water molecules present in the −2 layer of the *S. cerevisiae* SNARE complex. *D*, superposition of the −2 layers of the *S. cerevisiae* and neuronal SNARE complexes. *E*, simulated annealing omit map contoured at 3 σ of the water molecules present between the −4 and −5 layers of the *S. cerevisiae* SNARE complex. *F*, superposition of the −4 and −5 layers of the *S. cerevisiae* and neuronal SNARE complexes. *G*, ribbon diagram of the cavity region between the +5 and +6 layers of the *S. cerevisiae* SNARE complex. *H*, superposition of the +5 and +6 layers of the *S. cerevisiae* and neuronal SNARE complexes.

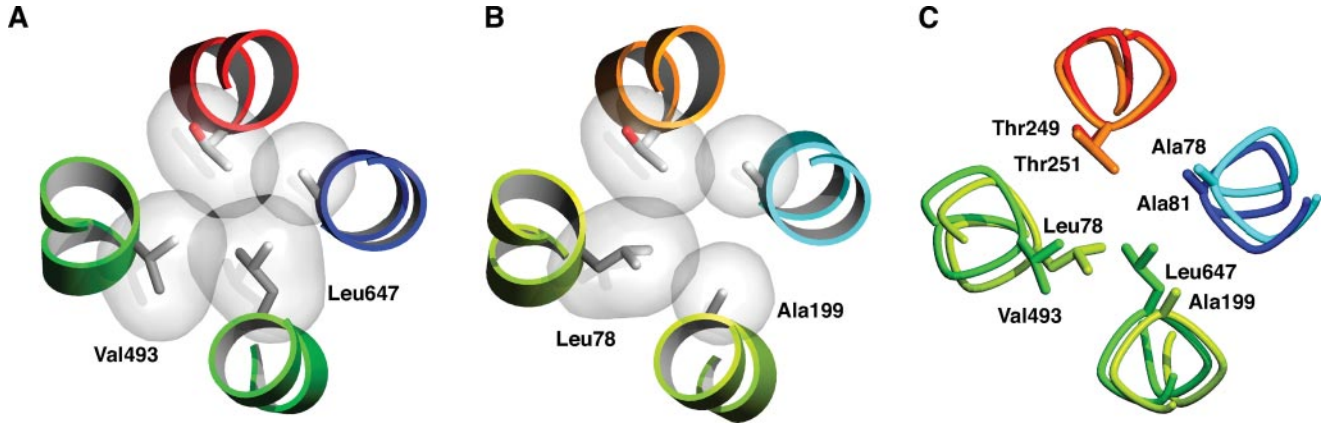

FIGURE 6. **Packing in the +7 layer.** Snc1p is shown in *blue*, Ssop in *red*, Sec9p in *green*, synaptobrevin 2 in *cyan*, syntaxin 1A in *orange*, and SNAP-25A in *yellow*. *A*, packing of the +7 layer in the *S. cerevisiae* plasma membrane SNARE complex. The side chains are shown in *stick* representation with transparent surfaces. *B*, packing of the +7 layer in the neuronal plasma membrane SNARE complex. *C*, superposition of the *S. cerevisiae* and neuronal SNARE complex +7 layer.

2 °C. The combined removal of all three cavities stabilizes the *S. cerevisiae* SNARE complex by 6.7 °C (Fig. 4).

The electrostatic potentials of all SNARE complexes solved to date are very negative in the center region (11) (Fig. 5). The overall charge of the neuronal SNARE complex (PDB code 1N7S) is −19, whereas the overall charge of the *S. cerevisiae* SNARE complex presented here is −11. The early and late endosomal SNARE complexes (PDB codes 2NPS and 1GL2) have overall charges of −9 and −18, respectively.

The negative electrostatic potential of the center region of the neuronal SNARE complex is thought to be important for interaction with the Ca^{2+} sensor synaptotagmin I (21). Synaptotagmin I has a positively charged surface, especially in the presence of Ca^{2+} (22). The interaction between synaptotagmin I and SNARE complex can be disrupted by increasing the salt concentrations above physiological levels (4), further supporting the importance of electrostatic interactions in the formation of the SNARE-synaptotagmin complex. It is unknown whether the negative surfaces present in the *S. cerevisiae* and endosomal SNARE complexes are structural features of SNARE proteins or if they are also involved in protein-protein interactions with other regulatory partners such as calmodulin (23).

The +7 layer of the SNARE complex has been proposed to be one of the key differences between SNARE complexes that fuse constitutively and those that undergo triggered fusion (24). For *Drosophila* SNAREs, the T254I mutation enhances both constitutive and evoked neurotransmitter release, suggesting that the tighter packing of isoleucine promotes SNARE formation and fusion, whereas the presence of threonine prevents good packing (Fig. 6*B*) and halts full SNARE complex formation. However, the plasma membrane yeast SNARE Sso1p contradicts this simple rule because it is involved in constitutive fusion and yet it has a threonine in the equivalent position (Thr-249). The structure of the *S. cerevisiae* SNARE complex shows that the +7 layer is well packed despite the presence of threonine (Fig. 6*A*): The Sec9p valine (Val-493) and leucine (Leu-647), Snc1p Ala-78, and Sso1p Thr249 form a well-packed layer (Fig. 6*C*). Thus, rather than a particular residue, it is the combination of residues that determines the packing in the +7 layer and perhaps contributes to the difference between constitutive and triggered fusion.

SNARE proteins play an important role in vesicle trafficking, which is a fundamental process in all eukaryotic cells for the transfer of proteins, lipids, and metabolites between compartments. Because of the importance of these processes, the SNARE complex has remained conserved throughout evolution. Here we have shown that the *S. cerevisiae* SNARE complex is structurally similar to SNARE complexes from higher eukaryotes but exhibits more pronounced bending near the ionic layer and contains water-filled cavities. These cavities are in part contributing to the decreased stability of the *S. cerevisiae* plasma membrane SNARE complex.

Acknowledgments—We thank Tim D. Fenn for helpful discussions and reading of the manuscript. This work is based on research conducted at the Stanford Synchrotron Radiation Laboratory, a national user facility operated by Stanford University on behalf of the United States Department of Energy, Office of Basic Energy Sciences. The SSRL Structural Molecular Biology Program is supported by the Department of Energy Office of Biological and Environmental Research, by the National Institutes of Health National Center for Research Resources, Biomedical Technology Program, and NIGMS, National Institutes of Health.

REFERENCES

1. Brunger, A. T. (2006) *Q. Rev. Biophys.* **38,** 1–47
2. Jahn, R., and Scheller, R. H. (2006) *Nat. Rev. Mol. Cell Biol.* **7,** 631–643
3. Rizo, J., and Sudhof, T. C. (2002) *Nat. Rev. Neurosci.* **3,** 641–653
4. Tang, J., Maximov, A., Shin, O. H., Dai, H., Rizo, J., and Sudhof, T. C. (2006) *Cell* **126,** 1175–1187
5. Gerber, S. H., and Sudhof, T. C. (2002) *Diabetes* **51,** Suppl. 1, S3–S11
6. Mayer, A. (2002) *Annu. Rev. Cell Dev. Biol.* **18,** 289–314
7. Bonifacino, J. S., and Glick, B. S. (2004) *Cell* **116,** 153–166
8. Fasshauer, D., Otto, H., Eliason, W. K., Jahn, R., and Brunger, A. T. (1997) *J. Biol. Chem.* **272,** 28036–28041
9. Rice, L. M., Brennwald, P., and Brunger, A. T. (1997) *FEBS Lett.* **415,** 49–55
10. Ernst, J. A., and Brunger, A. T. (2003) *J. Biol. Chem.* **278,** 8630–8636
11. Sutton, R. B., Fasshauer, D., Jahn, R., and Brunger, A. T. (1998) *Nature* **395,** 347–353
12. Zwilling, D., Cypionka, A., Pohl, W. H., Fasshauer, D., Walla, P. J., Wahl, M. C., and Jahn, R. (2007) *EMBO J.* **26,** 9–18

13. Antonin, W., Fasshauer, D., Becker, S., Jahn, R., and Schneider, T. R. (2002) *Nat. Struct. Biol.* **9,** 107–111
14. Otwinowski, Z., and Minor, W. (1997) *Methods Enzymol.* **276,** 307–326
15. McCoy, A. J., Grosse-Kunstleve, R. W., Storoni, L. C., and Read, R. J. (2005) *Acta Crystallogr. Sect. D Biol. Crystallogr.* **61,** Pt. 4, 458–464
16. Emsley, P., and Cowtan, K. (2004) *Acta Crystallogr. Sect. D Biol. Crystallogr.* **60,** Pt. 12, Pt. 1, 2126–2132
17. Brunger, A. T., Adams, P. D., Clore, G. M., DeLano, W. L., Gros, P., Grosse-Kunstleve, R. W., Jiang, J. S., Kuszewski, J., Nilges, M., Pannu, N. S., Read, R. J., Rice, L. M., Simonson, T., and Warren, G. L. (1998) *Acta Crystallogr. Sect. D Biol. Crystallogr.* **54,** Pt. 5, 905–921
18. Adams, P. D., Grosse-Kunstleve, R. W., Hung, L. W., Ioerger, T. R., McCoy, A. J., Moriarty, N. W., Read, R. J., Sacchettini, J. C., Sauter, N. K., and Terwilliger, T. C. (2002) *Acta Crystallogr. Sect. D Biol. Crystallogr.* **58,** Pt. 11, 1948–1954
19. Laskowski, R. A., Rullmannn, J. A., MacArthur, M. W., Kaptein, R., and Thornton, J. M. (1996) *J. Biomol. NMR* **8,** 477–486
20. Antonin, W., Holroyd, C., Fasshauer, D., Pabst, S., Von Mollard, G. F., and Jahn, R. (2000) *EMBO J.* **19,** 6453–6464
21. Rizo, J., Chen, X., and Arac, D. (2006) *Trends Cell Biol.* **16,** 339–350
22. Shao, X., Li, C., Fernandez, I., Zhang, X., Sudhof, T. C., and Rizo, J. (1997) *Neuron* **18,** 133–142
23. Peters, C., and Mayer, A. (1998) *Nature* **396,** 575–580
24. Lagow, R. D., Bao, H., Cohen, E. N., Daniels, R. W., Zuzek, A., Williams, W. H., Macleod, G. T., Sutton, R. B., and Zhang, B. (2007) *PLoS Biol.* **5,** e72
25. Fenn, T., Ringe, D., and Petsko, G. (2003) *J. Applied Crystallogr.* **36,** 944–947
26. DeLano, W. (2002) The PyMOL Molecular Graphics System, DeLano Scientific LLC, San Carlos, CA
27. Brunger, A. T. (2007) *Nature Protocols* **2,** 2728–2733